Pan-cancer mutational landscape of the PPAR pathway reveals universal patterns of dysregulated metabolism and interactions with tumor immunity and hypoxia

Short title: Pan-cancer PPAR signature

Wai Hoong Chang and Alvina G. Lai

Nuffield Department of Medicine, University of Oxford,

Old Road Campus, Oxford, OX3 7FZ, United Kingdom

For correspondence: Alvina.Lai@ndm.ox.ac.uk; alvinagracelai@gmail.com

Abstract:

Peroxisome proliferator-activated receptors (PPARs) are a family of nuclear receptors that regulate lipid metabolism and bioenergetic demands within living systems. Consequently, aberrant expression of PPAR genes could predispose individuals to diseases including cancer. PPAR signaling exerts pleiotropic functions in cancer, yet, little is known about the interactions between genetic and transcriptional events of pathway genes in a pan-cancer context. Employing multidimensional datasets of over 18,000 patients involving 21 cancers, we performed systematic characterization on copy number alteration and differential transcript expression of 74 PPAR pathway genes. We identified 18 genes demonstrating mutually exclusive patterns of loss- and gain-of-function phenotypes. These genes successfully predicted patient survival rates in bladder, renal, glioma, liver and stomach/esophageal cancers. Dysregulated PPAR signaling in these cancers converged on common downstream pathways associated with multiple metabolic processes. Moreover, clinically-relevant relationships between PPARs and hypoxia were observed where hypoxia further aggravates disease phenotypes in tumor subtypes with aberrant PPAR signaling. In glioma samples, including astrocytoma and oligoastrocytoma, PPAR hyperactivation is associated with immunosuppression through increased regulatory T cell expression. Our analysis reveals underappreciated levels of diversity and conservation in PPAR genes that could lay the groundwork for therapeutic strategies targeting tumor metabolism, immunity and hypoxia.

Keywords:

PPAR; metabolism; hypoxia; tumor immunity; glioma; pan-cancer

Introduction:

A series of genetic and phenotypic changes must take place during malignant transformation to rewire cellular programs and signal transduction pathways into a permissive state that facilitates tumor survival. Metabolic reprogramming, which occurs through the attainment of genetic and epigenetic mutations, is often a critical step in tumorigenesis because cancer cells have a unique requirement for increase glucose uptake and lactate fermentation even in the presence of oxygen[1,2]. Tumor cells also have increased fatty acid oxidation and turnover[3], and this is perhaps not unforeseen because fatty acids yield twice as much energy as glucose. Tumor cells with increased *de novo* fatty acid synthesis through the upregulation of fatty acid synthase are also often more aggressive[4]. Fatty acid oxidation is activated by upstream effectors involving signal transduction pathways such as peroxisome proliferator-activated receptor (PPAR) and AMP-activated protein kinase[2,5]. Given their bioenergetic dependence on fatty acid oxidation, a better understanding of how lipid pathways are dysregulated in cancer cells will be crucial for successful therapy.

PPARs are a family of nuclear receptor transcription factors involved in regulating metabolic homeostasis whose activity is regulated by fatty acid ligands[6]. Three categories of PPARs have been identified in humans; PPARα, PPARβ/δ, and PPARγ. Once activated, PPARs heterodimerize with retinoid X receptors (RXRs) to regulate the expression of downstream target genes harboring peroxisome proliferator response element motifs. Given the availability of PPAR agonists and antagonists, investigations on the role of PPAR signaling in cancer has begun to gain momentum. PPAR agonists may promote or suppress tumor formation depending on the cellular context. PPARγ agonists such as pioglitazone and troglitazone are effective inhibitors of cell growth in colorectal[7–9], melanoma[10] and ovarian cancers[11]. PPARγ agonists could also inhibit the proliferation and induce cell cycle arrest in brain tumor stem cells in a dose-dependent manner[12]. In contrast, treatment with a PPARγ antagonist depletes tumorsphere formation in $ERBB2^{+}$ breast cancer stem cells, suggesting that PPARγ is

essential for breast cancer stem cell maintenance[13]. PPARδ is also required for hematopoietic stem cell maintenance, and its inhibition prevents asymmetrical cell division required for stem cell self-renewal[14].

The ubiquitous impact of PPAR signaling across diverse cancer types necessitates a systematic curation of genomic and transcriptomic alterations of all PPAR pathway genes using a pan-cancer approach, which may offer unprecedented insights into elucidating novel druggable targets. We performed an integrated analysis on PPAR pathway genes using genomic, transcriptomic and clinical data from 18,484 patients involving 21 cancer types (Fig. 1A). We discovered common and distinct patterns of genetic mutations and dysregulated transcript expression converging on a core set of 18 genes that harbor clinically-relevant prognostic information in multiple cancer types. Given its pervasive influence in numerous biological processes, we also examined the crosstalk between PPAR signaling and tumor hypoxia or tumor immunity. Oncogenic variants of the PPAR pathway identified in this study can be integrated into current initiatives on personalized therapy employing PPAR agonists to target fatty acid metabolism in conjunction with first-line treatments.

Materials and Methods:

Gene set and cancer cohorts:

Seventy-four PPAR pathway genes were retrieved from the Kyoto Encyclopedia of Genes and Genomes (KEGG) database listed in Table S1. Transcriptomic, genomic and clinical datasets of 21 cancer types generated by The Cancer Genome Atlas (TCGA) were retrieved from the Broad Institute GDAC Firehose website[15].

Somatic copy number alterations analyses:

GISTIC Level 4 copy number variation profiles for each cancer type were downloaded from Firehose. To determine gene amplifications and deletions, we utilized GISTIC gene-level tables that provided discrete amplification and deletion indicators[16]. Samples with GISTIC values higher than the maximum copy-ratio for each chromosome arm (> +2) were annotated as 'deep amplification' events. In contrast, samples with values lower than the minimum copy-ratio for each chromosome arm (< -2) were annotated as 'deep deletion' events. Samples with GISTIC values of +1 and -1 were annotated as 'shallow amplifications' and 'shallow deletions' respectively.

Determining PPAR, hypoxia and regulatory T cell (Treg) scores:

An 18-gene signature of PPAR signaling is developed from putative loss- or gain-of-function genes. Loss-of-function genes were identified from genes that were recurrently deleted and downregulated in tumors. Gain-of-function genes were identified from genes that were recurrently amplified and upregulated in tumors. We calculated 18-gene scores for each patient by taking the average expression of *APOA1, PPARA, ACOX2, ANGPTL4, FABP3, PLIN2, AQP7, ACSL1, FABP5, ACADL, PLIN5, PPARG, ACADM, GK, CPT2, SCP2, ACAA1,* and *PCK2*. Hypoxia scores were calculated from the average expression of 52-computationally-derived hypoxia-responsive genes[17]. Treg scores were determined from the expression of 31 Treg genes identified from the overlap of four Treg signatures[18–21].

Differential expression and survival analyses:

We have published detailed methods on both types of analyses[22]; hence they will not be repeated here. Briefly, differential expression analyses on 74 PPAR pathway genes were performed on tumor and non-tumor samples. Differential expression analyses were also performed between the 4th and 1st quartile patients stratified using the 18-gene signature. Survival analyses were performed using the Kaplan-Meier method coupled with log-rank tests, Cox proportional hazards regression and receiver operating characteristics. For figures 5 and 6, Spearman's correlation analyses were performed to determine the relationship between PPAR signaling and tumor hypoxia or Treg expression. Patients were separated into four categories based on median PPAR 18-gene scores and hypoxia or Treg scores for Kaplan-Meier and Cox regression analyses. Circular heatmaps in figure 7 were generated based on 18-gene scores in glioma patients ranked in decreasing order from high (purple) to low (yellow). Immune checkpoint genes (*PD1, PDL1, PDL2, CTLA4*, and *CD276*) were sorted according to decreasing 18-gene scores for heatmap generation.

KEGG enrichment, Gene Ontology (GO) and transcription factor analyses:

Differentially expressed genes (DEGs) from 4th vs. 1st quartile patients were used for pathway analyses using GeneCodis[23] and Enrichr[24,25]. DEGs were mapped to KEGG and GO databases to identify significantly enriched pathways. DEGs were mapped to ChEA and ENCODE databases to identify transcription factors involved in regulating the DEGs.

All plots were generated using R packages (pheatmap, ggplot2, and GOplot). The Venn diagram was generated using InteractiVenn[26].

Results:

Somatic copy number alterations of PPAR pathway genes reveal conserved mutations that were recurrently amplified or deleted

We retrieved 74 genes implicated in PPAR signaling from the KEGG database along with genomic, transcriptomic and clinical data representing 21 major cancer types (n=18,484) from TCGA (Fig. 1A; Table S2). We analyzed somatic copy number alteration (SCNA) events of the 74 genes in these cancer types and observed that lung squamous cell carcinoma (LUSC) and papillary renal cell carcinoma (KIRP) had the highest and lowest fraction of samples with deleted PPAR pathway genes respectively (Fig. 1B). When considering gene amplification, the highest and lowest fraction of samples with amplified genes were observed in esophageal carcinoma (ESCA) and pancreatic adenocarcinoma (PAAD) respectively (Fig. 1B).

To identify genes that exhibited similar patterns of recurrent deletion or amplification across cancers, we interrogated SCNA profiles that were present in at least 20% of samples per cancer type in at least one-third of cancer types (> 7 cancers). Using these criteria, we identified 51 and 25 genes that were recurrently lost (Fig. 1C) and gained (Fig. 1D) respectively. All 51 genes were found to be deleted in at least 20% of samples in esophageal carcinoma (ESCA) and lung squamous cell carcinoma (LUSC) (Fig. 1C). In contrast, only 2 out of 51 genes (*CPT1B* and *PPARA*) were recurrently deleted in papillary renal cell carcinoma (KIRP) (Fig. 1C). Again, esophageal carcinoma (ESCA) emerged with the highest number of recurrently amplified genes (24 out of 25 genes) while only 3 out of 25 genes (*PCK1, PLTP*, and *CD36*) were recurrently amplified in glioma (GBMLGG) (Fig. 1D). Further examination into individual genes revealed that *LPL* was the most deleted gene found in 17 cancer types, followed by *AQP7, CPT1B, ME1, PLIN2, PPARA* and *SCD* that were each recurrently deleted in 16 cancer types (Fig. 1C). In contrast, *NR1H3, PDPK1, RXRB,* and *SLC27A1* were some of the least deleted genes found only in 7 cancer types (Fig. 1C). *PCK1* and *PLTP* were both

amplified in all 21 cancers, and four other genes (*CD36, CYP7A1, FABP4*, and *FABP5*) were found to be amplified in at least 16 cancer types (Fig. 1D).

We reasoned that SCNA events associated with transcript upregulation or downregulation might represent candidate gain-of-function or loss-of-function genes. Genes that were concomitantly deleted and downregulated could indicate loss-of-function. Moreover, gain-of-function phenotypes can be predicted from genes that were concurrently amplified and overexpressed. When overlaid with mutation data, differential expression analyses performed between tumor and non-tumor samples identified 43 genes that conformed to these criteria. A total of 38 genes were recurrently deleted and downregulated (log_2 fold-change < -0.5, $P < 0.05$) in at least 7 cancer types: *LPL, AQP7, ME1, PLIN2, PPARA, ACSL1, SORBS1, ACOX2, CYP8B1, FABP2, FABP3, PCK2, RXRA, SCD5, ACAA1, APOA1, APOA5, APOC3, SLC27A2, SLC27A4, ACOX3, ACSBG2, ANGPTL4, GK, ILK, PLIN4, PLIN5, PPARG, ACSBG1, ACSL6, CPT2, CYP4A22, SCP2, SLC27A6, ACADM, CYP4A11, ACADL,* and *CYP27A1* (Fig. 1C). Five genes were found to be amplified and upregulated (log_2 fold-change > 0.5, $P < 0.05$) in at least 7 cancer types: *FABP5, APOA2, OLR1, CPT1C,* and *FABP6* (Fig. 1D). These genes were subsequently prioritized as pan-cancer PPAR gain-of-function and loss-of-function genes.

Prognostic significance of highly-correlated PPAR mutations in six diverse cancer types

Given the widespread patterns of genomic and transcriptomic alterations of PPAR pathway genes, we reasoned that these features would be significantly associated with patient survival outcomes. Employing Cox proportional hazards regression, we examined the prognostic roles of all 43 genes identified previously. Except for *ACSBG2*, all genes harbored prognostic information in at least one cancer type (Fig. 2A). Interestingly, the glioma cohort has the

highest number of prognostic genes (30 out of 43) (Fig. 2A). We performed Spearman's correlation analyses on hazard ratios (HR) retrieved from Cox regression analyses to reveal prognostic genes that symbolize pan-cancer significance. We identified 18 highly-correlated genes in this manner and considered them as a pan-cancer PPAR signature: *APOA1, PPARA, ACOX2, ANGPTL4, FABP3, PLIN2, AQP7, ACSL1, FABP5, ACADL, PLIN5, PPARG, ACADM, GK, CPT2, SCP2, ACAA1* and *PCK2* (Fig. 2B). We next quantified the extent of PPAR signaling by generating a summary score for each patient based on the average expression of the 18 genes. On average, liver (LIHC) and head and neck cancers (HNSC) had the highest and lowest levels of PPAR activity respectively (Fig. 2C). When employing the 18-gene scores for patient stratification, we observed that levels of PPAR signaling conferred prognostic information in six cancer cohorts (Fig. 2D and 2E). Interestingly, the significance of PPAR signature genes in determining overall survival is cancer-type dependent. Kaplan-Meier analyses on patients within the 1st and 4th survival quartiles demonstrated that elevated PPAR signaling was significantly correlated with poor prognosis in patients with glioma (P<0.0001) and stomach and esophageal cancers (P=0.0078) (Fig. 2D). On the contrary, high expression of signature genes was associated with better survival outcomes in bladder (P=0.031), pan-kidney (consisting of clear cell renal cell, chromophobe renal cell and papillary renal cell carcinoma; P=0.041), clear cell renal cell (P=0.0027) and liver cancer (P=0.0029) cohorts (Fig. 2D). Univariate Cox regression analyses confirmed that patients with high 18-gene scores (4th quartile) had significantly higher death risks in glioma (HR=6.899, P<0.0001) and stomach and esophageal cancers (HR=1.623, P=0.0084) (Table S3). Likewise, in cancers where PPAR signaling is associated with good outcomes, Cox regression analyses confirmed that patients with high 18-gene scores (4th quartile) had improved overall survival rates, which support the hypothesis on the tumor-attenuating effects of PPAR signaling in these cancers: bladder (HR=0.578, P=0.033), pan-kidney (HR=0.687, P=0.032), clear cell renal cell (HR=0.543, P=0.0041) and liver (HR=0.403, P=0.0063) (Table S3).

The 18-gene signature is an independent predictor of survival

The tumor, node, and metastasis (TNM) staging system is frequently used in cancer prognostication. To determine whether the signature was confounded by TNM staging, we performed multivariate Cox regression analyses and found that the PPAR signature remained an independent predictor of overall survival: bladder (HR=0.692, P=0.031), pan-kidney (HR=0.625, P=0.012), clear cell renal cell (HR=0.604, P=0.018), liver (HR=0.492, P=0.035) and stomach and esophageal (HR=1.509, P=0.033) (Table S3). Since the signature was independent of TNM stage, we predict that it could be used to improve the sensitivity and specificity of TNM staging. We employed receiver operating characteristic (ROC) analyses to compare the predictive performance of the signature with a combined model that unites the signature with TNM staging. ROC analyses revealed that the combined model (signature + TNM staging) had higher area under the curve (AUC) values: bladder (0.722 vs. 0.697), pan-kidney (0.811 vs. 0.720), clear cell renal cell (0.813 vs. 0.722), liver (0.745 vs. 0.679) and stomach and esophageal (0.667 vs. 0.601) (Fig. 3B). Moreover, Kaplan-Meier analyses and log-rank tests revealed that the signature offered an additional resolution to further separate similarly-staged tumors: bladder (P<0.0001), pan-kidney (P<0.0001), clear cell renal cell (P<0.0001), liver (P<0.0001) and stomach and esophageal (P<0.0001) (Fig. 3A).

Hyperactivation of PPAR signaling is associated with adverse survival outcomes in glioma patients. Glioma samples are categorized into four histological subtypes: low-grade gliomas (astrocytoma, oligoastrocytoma, and oligodendroglioma) and grade IV glioblastoma multiforme. Kaplan-Meier analyses confirmed that elevated PPAR signaling was indeed associated with poor survival outcomes in astrocytoma (P=0.0011), oligoastrocytoma (P=0.016) and glioblastoma multiforme (P=0.00014) (Fig. 3A). These observations were independently confirmed by Cox regression analyses where patients within the 4^{th} quartile had higher mortality rates: astrocytoma (HR=3.204, P=0.0019), oligoastrocytoma (HR=4.232, P=0.027) and glioblastoma multiforme (HR=2.699, P=0.00023) (Table S3). ROC analyses revealed that the predictive performance of the signature was the best in astrocytoma

(AUC=0.844), followed by oligoastrocytoma (AUC=0.833) and glioblastoma multiforme (AUC=0.729) (Fig. 3B). The signature also performed well when all histological subtypes (including oligodendroglioma) were considered as a group (AUC=0.832) (Fig. 3B).

The 18-gene signature reveals aberration in oncogenic pathways converging on similar downstream targets associated with deranged metabolism

Since aberration in PPAR signaling is linked to clinical outcomes (Fig. 2 and 3), we hypothesized that the function of signature genes in these cancers might converge on similar downstream targets. To identify oncogenic targets associated with PPAR signaling, we performed differential expression analyses between patients separated into 4^{th} and 1^{st} quartiles based on their 18-gene scores. The highest number of differentially expressed genes (DEGs; $-1.5 > \log_2$ fold change > 1.5; $P<0.01$) was observed in glioma (2,240 genes), followed by liver (1,578 genes), bladder (1,374 genes), stomach and esophageal (1,323 genes), pan-kidney (897 genes) and clear cell renal cell (721 genes) (Fig. 4A; Table S4). Remarkably, we observed overlaps in downstream transcriptional targets resulting from aberrant PPAR signaling in these cancers despite their distinct pathologies; 23 genes were found to be dysregulated in at least five cohorts, 249 genes in at least four cohorts and 739 genes in at least three cohorts (Fig. 4A; Table S4). Together, these implied that PPAR signaling plays a conserved role in driving oncogenic progression. We performed Gene Ontology (GO) and KEGG enrichment analyses to further assess the functional significance of the DEGs (Table S4). All six cancer cohorts exhibited very similar patterns of enriched biological processes and oncogenic pathways (Fig. 4B and 4C). Biological functions associated with metabolism, cell adhesion, and cell-to-cell signaling were among some of the most enriched processes (Fig. 4B). Moreover, KEGG analyses showed that numerous metabolic-related pathways were dysregulated in patients with altered PPAR signaling (Fig. 4C), which provided an independent confirmation of the functional significance of the PPAR pathway in lipid and fatty acid

metabolism. Together, these results suggest that altered PPAR signaling may cause metabolic reprogramming of tumor cells to impact patient survival directly. To determine which transcription factors (TFs) were upstream regulators of the DEGs, we mapped the DEGs to ENCODE and ChEA databases using the Enrichr tool. Interestingly, DEGs from all six cohorts were enriched for binding targets of SUZ12 and EZH2, which are important regulators of cancer stem cells (CSCs) (Fig. 4D). Enrichments of other TFs implicated in CSC maintenance, RE1 Silencing Transcription Factor (REST) and SMAD4, were also observed, implying the underappreciated connection between PPAR signaling and self-renewal mechanisms (Fig. 4D).

Crosstalk between PPAR signaling and other pro-anabolic pathways such as mTOR/PI3K/AKT and pro-catabolic pathways such as AMPK have been reported[27,28]. To investigate potential associations between PPAR and mTOR/PI3K/AKT signaling, we calculated mTOR/PI3K/AKT scores using the following equation: mTOR/PI3K/AKT score = AKT + mTOR + GSK3 + S6K + S6 – PTEN[29]. PPAR hyperactivation was associated with poor survival outcomes in patients with glioma while in bladder cancer, high PPAR scores were linked to better outcomes (Fig. 2). Interestingly, when PPAR and mTOR scores were combined as a single model for survival analyses, we observed that glioma patients with high mTOR and high PPAR scores performed the worst (Fig. S1). In contrast, since PPAR hyperactivation was associated with good prognosis in patients with bladder cancer, patients with low mTOR and low PPAR scores had the worst outcomes (Fig. S1). This suggests that two anabolic pathways (PPAR and mTOR) could synergize to influence prognosis.

Since PPAR plays an anabolic role in lipid synthesis and AMPK inhibits anabolic processes, we performed correlation analyses between the 18 PPAR signature genes and seven AMPK genes encoding α, β and γ subunits (*PRKAA1, PRKAA2, PRKAB1, PRKAB2, PRKAG1, PRKAG2* and *PRKAG3*). Remarkably, we observed that the expression of a majority of PPAR signature genes negatively correlated with AMPK genes – this is especially true for bladder,

glioma, clear cell renal cell and liver cancers (Fig. S2). These results support the overarching view that AMPK functions to decrease anabolic processes such as PPAR-associated lipid anabolism where in tumors with elevated PPAR signaling, we would expect to see decreased AMPK gene expression (Fig. S2).

Tumor hypoxia worsen survival outcomes in patients with impaired PPAR signaling

Hypoxia is a universal feature in almost all solid malignancies due to the formation of aberrant tumor microvasculature[30–33]. As an adaptation strategy to hypoxic environments, tumor cells need to reprogram their metabolic requirements to survive[34]. Since PPARs are critical metabolic regulators, we predict that tumor hypoxia would influence the behavior of PPAR pathway genes and consequently patient prognosis. To evaluate the contribution of tumor hypoxia on PPAR signaling, we assessed the levels of hypoxia in each patient using a hypoxia gene signature where hypoxia scores were calculated from the mean expression values of 52 hypoxia-responsive genes[17]. PPAR scores were significantly positively correlated with hypoxia scores in glioma (rho=0.64, P<0.0001) and pan-kidney (rho=0.24, P<0.0001) cohorts (Fig. 5A). However, this trend was reversed in liver (rho= -0.47, P<0.0001) and stomach and esophageal cancers (rho= -0.20, P<0.0001) (Fig. 5A). Patients were grouped into four categories based on their median PPAR and hypoxia scores for survival analyses. Intriguingly, the joint relationship between hypoxia and PPAR signaling allowed further delineation of risk groups that influenced survival outcomes: glioma (full cohort; P<0.0001), astrocytoma (P<0.0001), oligoastrocytoma (P=0.001), pan-kidney (P<0.0001), liver (P=0.0007) and stomach and esophageal (P=0.039) (Fig. 5B). According to analyses in the previous section, high 18-gene PPAR scores can either be associated with poor or good outcomes depending on the cancer type (Fig. 2). In cancers where a high PPAR score is associated with poor outcomes, a high hypoxia score would further exacerbate disease phenotypes in these patients: glioma (full cohort; HR=7.938, P<0.0001), astrocytoma (HR=7.380, P<0.0001),

oligoastrocytoma (HR=14.179, P=0.011) and stomach and esophageal (HR=1.748, P=0.0058) (Fig. 5C). On the other hand, high PPAR score is a good prognostic factor in renal and liver cancers. Hence, patients with both low PPAR and high hypoxia scores would have the highest mortality rates: pan-kidney (HR=3.187, P<0.0001) and liver (HR=2.849, P=0.00014) (Fig. 5C).

Haider et al. previously demonstrated that pan-cancer genetic alterations in metabolic genes are associated with hypoxia-mediated shift in tumor metabolism[34]. They proposed a set of 44 metabolic driver genes that were significantly associated with hypoxia. To further support our results on the PPAR-hypoxia crosstalk, we calculated 44-gene scores for each patient by taking the average expression of *PYCR3, ALG3, NUDT1, PSPH, FLAD1, CLCN2, GGH, SLC39A4, TPI1, TSTA3, UCK2, GPI, GAPDH, PYCR1, TK1, LPCAT1, FLVCR1, SRD5A1, SLC25A10, NME1, DHRS13, SLC5A6, SQLE, SLC12A8, ABCC5, GMPS, KCNMB3, SLC25A13, SLC4A2, PDE7A, UCKL1, AHCY, IMPDH1, CYC1, EDEM2, ITPA, DHTKD1, PIGU, B4GALT3, HCN3, SLC39A11, TTYH3, DHCR7* and *TYMS*[34]. Correlation analysis between PPAR scores and 44-gene-hypoxia-metabolic scores in patients with glioma revealed a significant association (rho=0.3, P<0.0001) (Fig. S3A). Moreover, when both PPAR and 44-gene scores were combined as a single model for survival analysis, patients within the high-PPAR and high-44-gene-score category performed the worst (Fig. S3B, C). Taken together, these results suggest a model whereby PPAR signaling may influence transcriptional targets of hypoxia (Fig. 5) and that tumors with hypoxia-associated metabolic dysregulation, as measured by the 44-gene signature (Fig. S3), also had elevated PPAR signaling.

Immuno-oncogenic properties of PPAR signature genes in patients with glioma.

It was reported recently that focal amplification and overexpression of PPARγ inhibits the secretion of inflammatory cytokines and reduces cytotoxic $CD8^+$ T-cell infiltration[35]. PPARγ and RXRA activities promote resistance to immune checkpoint blockade to create an environment that favors tumor growth[35]. In order to evaluate the role of PPAR signaling in modulating tumor immunity, we first needed to identify genes that are associated with immunosuppression. We retrieved four regulatory T cell (Treg) gene signatures[18–21] and looked for genes that were common in all four signatures. We identified 31 genes that were present in all four signatures to yield a more representative Treg gene set that is not specific to single tumor type. We calculated Treg scores for each patient based on the average expression of the 31 genes. A strong positive correlation between Treg and PPAR 18-gene scores (rho=0.65, P<0.0001) was observed in glioma patients, suggesting that tumor cells with elevated PPAR signaling were hypoimmunogenic (Fig. 6A). Patients were stratified into four categories based on median PPAR and Treg scores for survival analyses. Intriguingly, high expression of Treg genes would further promote disease aggression in glioma tumors with hyperactive PPAR signaling (HR=7.356, P<0.0001) (Fig. 6B and 6C). This observation was repeated in glioma histological subtypes: astrocytoma (HR=3.699, P<0.0001) and oligoastrocytoma (HR=3.227, P=0.038) (Fig. 6B and 6C). Taken together, metabolic reprogramming of the tumor microenvironment through PPAR signaling may influence anti-tumor immunity and consequently immunotherapeutic outcomes in clinical settings. Indeed, we observed that PPAR signaling is significantly positively correlated with the expression profiles of canonical immune checkpoint markers, suggesting that pharmacological inhibition of PPAR could reinvigorate immunosurveillance in glioma patients; *PD1* (rho=0.41, P<0.0001), *PDL1* (rho=0.49, P<0.0001), *PDL2* (rho=0.62, P<0.0001), *CTLA4* (rho=0.38, P<0.0001) and *CD276* (rho=0.36, P<0.0001) (Fig. 7C).

Discussion:

In an integrated analysis involving multidimensional datasets from TCGA, we examined molecular characteristics of the PPAR pathway comprising of 74 genes across 18,484 patients representing 21 cancer types. We started by cataloging genes with significant SCNA patterns linked to transcriptional dysregulation. We uncovered tissue-specific and universal mutation profiles that resulted in gene upregulation or silencing, which highlight novel oncogenic mechanisms of PPAR signaling that has been previously underappreciated. We identified a set of highly correlated genes (18-gene signature) that were consistently associated with survival outcomes across six cancer cohorts. In-depth analysis of differential PPAR signaling uncovered transcriptional perturbations of numerous signal-transduction pathways that were conserved among cancer types. Pathways associated with metabolic processes were among the most enriched ontologies; an observation that independently validates the role of PPARs in lipid transport, fatty acid oxidation, fatty acid catabolism and crosstalk with other lipogenic pathways[36].

Studies have demonstrated opposing effects of PPARs, whereby they could either promote or inhibit tumor growth. PPARδ, allows breast cancer cells to persist in severe metabolic environments; its expression level is negatively correlated with survival outcomes and increased metastatic ability of tumor cells in mice[37]. In pancreatic cancer, PPARδ represents a hub gene of a transcriptome-derived angiogenic network[38]. Suppression of PPARδ inhibits tumor growth and angiogenesis since its expression is positively correlated with tumor aggression, recurrent and metastasis[38]. *ANGPTL4* is a well-established PPARδ target gene. It promotes cell migration in colon cancer cells[39], lung metastasis in breast cancer[40] and venous invasion in colorectal and gastric cancers[41,42]. Moreover, inhibition of *ANGPTL4*, a downstream target of PPARδ, abrogates its pro-oncogenic effects and suppresses breast cancer cell invasion[43]. In our study, we identified *ANGPTL4* as one of the PPAR signature

412 genes. We found that the expression level of *ANGPTL4* is positively correlated with poor
413 survival outcomes in glioma, stomach and esophageal, lung, colon and renal cancers and
414 good survival outcomes in liver cancer (Fig. 2A; Fig. 7A). PPARs are highly pleiotropic since
415 they also possess anti-tumor functions. PPARγ induces apoptosis and inhibits tumor growth
416 in colon cancer cells[44]. PPARγ ligands impair gastric cancer cell proliferation in a dose-
417 dependent manner due to the upregulation of *p53* and downregulation of *cyclin E1* and tumor
418 burden in mice was reduced after treatment with a PPARγ agonist rosiglitazone[45]. Moreover,
419 overexpression of PPARγ inhibits the metastatic potential of gastric cancer cells through
420 attenuation of Wnt/β-Catenin signaling and *TERT* expression[46]. Our results demonstrate that
421 elevated expression of PPARγ is associated with better survival outcomes in renal and
422 bladder cancers, but poor survival outcomes in glioma (Fig. 2A; Fig. 7A). These striking cancer
423 type-dependent patterns further reinforce the benefit of our study, which investigates PPAR
424 pathway alterations in a larger pan-cancer context to expose diverse molecular complexities
425 and cancer-specific vulnerabilities.
426
427 Metabolic signals in the tumor microenvironment may regulate the behavior of immune cells
428 and affect patient response to immunotherapies. Immune cells possess unique metabolic
429 qualities and bioenergetic requirements[47]. Thus, alteration of the microenvironmental
430 metabolic landscape could have a direct impact on anti- or pro-tumor effects[47]. As lipid-
431 sensitive nuclear receptors, it is therefore not surprising that PPARs could modulate metabolic
432 homeostasis of immune cells. Indeed, multiple studies have shed light on the defining roles of
433 PPARs in regulating innate and adaptive immunity responses[48]. PPARγ activation in
434 macrophages stimulates lung cancer metastasis[49], while PPARδ activation promotes
435 apoptotic cell clearance[50]. PPARδ activation in myeloid cells promotes tumor invasion through
436 the activation of interleukin 10[51]. Also, dysregulated lipid metabolism and accumulation of fatty
437 acids in non-alcoholic fatty liver disease patients lead to increased oxidative damage, the loss
438 of $CD4^+$ T helper cells and impaired anti-tumor immunity in liver cancer[52]. A majority of patients

with muscle-invasive bladder cancer (MIBC) do not respond to immunotherapy. Korpal et al. found that immune evasion in MIBC patients is caused by PPARγ/RXRA overexpression, which inhibits inflammatory cytokine release[35]. Cytokine expression is restored through pharmacological inhibition of PPARγ[35]. Moreover, activation of LXRs (another member of the nuclear receptor superfamily involved in lipid homeostasis) inhibits neutrophil and dendritic cell migration into tumors contributing to tumor immunotolerance[53]. Our study may help prioritize PPAR candidates for future functional studies to pave the way for successful immunotherapeutic approaches.

Oxygen deprivation or hypoxia within the tumor microenvironment contributes to additional metabolic stress where hypoxia could drive the reprogramming of metabolic genes as an adaptation strategy for tumor survival[34]. We found that PPAR signaling can either be positively or negatively correlated with tumor hypoxia depending on cellular context (Fig. 7B). PPARγ expression and activity levels are downregulated under hypoxic conditions in human pulmonary artery smooth muscle cells leading to pulmonary hypertension[54]. PPARs could, in turn, regulate HIF-1a signaling in breast and ovarian cancer cell lines; treatment of these cells with a PPAR agonist before hypoxia incubation promotes HIF-1a degradation and suppresses VEGF secretion resulting in anti-tumor effects[55]. Curiously, another study reported that hypoxia elicited the downregulation of PPARα in intestinal epithelial cells[56] and since PPARα inhibits HIF-1a signaling, the absence of PPARα may be crucial for cells to mount an appropriate hypoxic response. We recently demonstrated that hypoxia also promotes the expression of Tregs and contributes to the impairment of anti-tumor surveillance to directly impact patient prognosis[22]. Hypoxia modulates angiogenic processes through regulating the function of immune cells. In natural killer cells, HIF-1a accumulation promotes tumor growth by inhibiting non-productive angiogenesis[57]. Hypoxia also promotes the angiogenic and immunosuppressive features of tumor-associated macrophages leading to tumor metastasis[58]. Immunosuppressive myeloid-derived suppressor cells are recruited to hypoxic

liver tumors and are blocked by HIF inhibitors to reestablish immune surveillance[59]. Further interrogation of the metabolism-hypoxia-immunity axis would provide a framework for combination therapeutic initiatives to simultaneously target these pathways.

In summary, we present a comprehensive catalog of genetic variants associated with PPAR signaling in over 18,000 tumor samples, including clinically actionable signature genes, which may serve as important foundations for understanding the wide-ranging effects of PPARs in tumorigenesis. Our study reveals candidate PPAR genes that may be used for personalized cancer treatment utilizing small molecule inhibitors or agonists targeting the PPAR pathway. Furthermore, the 18-gene signature could be used for patient stratification in cancer therapy involving hypoxia inhibitors and/or immune checkpoint blockade.

Competing interests: None declared.

Funding: None.

Availability of data and material: The datasets supporting the conclusions of this article are included within the article and its additional files.

Acknowledgment: Not applicable.

Authors' contributions: AGL designed the study, supervised the research and accepts responsibility for the integrity of the data analyzed. WHC and AGL analyzed the data, interpreted the results and wrote the initial manuscript draft. AGL revised the manuscript draft. All authors approved the final submitted manuscript.

References:

1 Liberti M V, Locasale JW. The Warburg effect: how does it benefit cancer cells? Trends Biochem Sci 2016;41:211–218.

2 Carracedo A, Cantley LC, Pandolfi PP. Cancer metabolism: fatty acid oxidation in the limelight. Nat Rev Cancer 2013;13:227.

3 Currie E, Schulze A, Zechner R, et al. Cellular fatty acid metabolism and cancer. Cell Metab 2013;18:153–161.

4 Flavin R, Peluso S, Nguyen PL, et al. Fatty acid synthase as a potential therapeutic target in cancer. Futur Oncol 2010;6:551–562.

5 la Cour Poulsen L, Siersbæk M, Mandrup S. PPARs: fatty acid sensors controlling metabolism. In: Seminars in cell & developmental biology. , 2012. p. 631–639.

6 Laganà A, Vitale S, Nigro A, et al. Pleiotropic actions of peroxisome proliferator-activated receptors (PPARs) in dysregulated metabolic homeostasis, inflammation and cancer: Current evidence and future perspectives. Int J Mol Sci 2016;17:999.

7 Qiao L, Dai Y, Gu Q, et al. Loss of XIAP sensitizes colon cancer cells to PPARγ independent antitumor effects of troglitazone and 15-PGJ2. Cancer Lett 2008;268:260–271.

8 Ban JO, Kwak DH, Oh JH, et al. Suppression of NF-κB and GSK-3β is involved in colon cancer cell growth inhibition by the PPAR agonist troglitazone. Chem Biol Interact 2010;188:75–85.

9 Yamauchi A, Takahashi I, Takasawa S, et al. Thiazolidinediones inhibit REG Iα gene transcription in gastrointestinal cancer cells. Biochem Biophys Res Commun 2009;379:743–748.

10 Smith AG, Beaumont KA, Smit DJ, et al. PPAR-gamma agonists attenuate proliferation and modulate Wnt/β-catenin signalling in melanoma cells. Int J Biochem Cell Biol 2009;41:844–852.

11 Yang Y-C, Tsao Y-P, Ho T-C, et al. Peroxisome proliferator-activated receptor-γ agonists cause growth arrest and apoptosis in human ovarian carcinoma cell lines. Int

J Gynecol Cancer 2007;17:418–425.

12 Chearwae W, Bright JJ. PPAR-gamma agonists inhibit growth and expansion of CD133+ brain tumour stem cells. Br J Cancer 2008;99:2044.

13 Wang X, Sun Y, Wong J, et al. PPARγ maintains ERBB2-positive breast cancer stem cells. Oncogene 2013;32:5512.

14 Ito K, Carracedo A, Weiss D, et al. A PML-PPAR-δ pathway for fatty acid oxidation regulates hematopoietic stem cell maintenance. Nat Med 2012;18:1350.

15 Weinstein JN, Collisson EA, Mills GB, et al. The cancer genome atlas pan-cancer analysis project. Nat Genet 2013;45:1113.

16 Mermel CH, Schumacher SE, Hill B, et al. GISTIC2. 0 facilitates sensitive and confident localization of the targets of focal somatic copy-number alteration in human cancers. Genome Biol 2011;12:R41.

17 Buffa FM, Harris AL, West CM, et al. Large meta-analysis of multiple cancers reveals a common, compact and highly prognostic hypoxia metagene. Br J Cancer 2010;102:428–435.

18 Zheng C, Zheng L, Yoo JK, et al. Landscape of Infiltrating T Cells in Liver Cancer Revealed by Single-Cell Sequencing. Cell 2017;169:1342-1356.e16.

19 De Simone M, Arrigoni A, Rossetti G, et al. Transcriptional Landscape of Human Tissue Lymphocytes Unveils Uniqueness of Tumor-Infiltrating T Regulatory Cells. Immunity 2016;45:1135–1147.

20 Plitas G, Konopacki C, Wu K, et al. Regulatory T cells exhibit distinct features in human breast cancer. Immunity 2016;45:1122–1134.

21 Tirosh I, Izar B, Prakadan SM, et al. Dissecting the multicellular ecosystem of metastatic melanoma by single-cell RNA-seq. Science (80-) 2016;352:189–196.

22 Chang WH, Forde D, Lai AG. A novel signature derived from immunoregulatory and hypoxia genes predicts prognosis in liver and five other cancers. J Transl Med 2019;17:14.

23 Tabas-Madrid D, Nogales-Cadenas R, Pascual-Montano A. GeneCodis3: a non-

546 redundant and modular enrichment analysis tool for functional genomics. Nucleic
547 Acids Res 2012;40:W478--W483.
548 24 Chen EY, Tan CM, Kou Y, et al. Enrichr: interactive and collaborative HTML5 gene list
549 enrichment analysis tool. BMC Bioinformatics 2013;14:128.
550 25 Kuleshov M V, Jones MR, Rouillard AD, et al. Enrichr: a comprehensive gene set
551 enrichment analysis web server 2016 update. Nucleic Acids Res 2016;44:W90--W97.
552 26 Heberle H, Meirelles GV, da Silva FR, et al. InteractiVenn: a web-based tool for the
553 analysis of sets through Venn diagrams. BMC Bioinformatics 2015;16:169.
554 27 Herzig S, Shaw RJ. AMPK: guardian of metabolism and mitochondrial homeostasis.
555 Nat Rev Mol cell Biol 2018;19:121.
556 28 Cairns RA, Harris IS, Mak TW. Regulation of cancer cell metabolism. Nat Rev Cancer
557 2011;11:85.
558 29 Creighton CJ, Fu X, Hennessy BT, et al. Proteomic and transcriptomic profiling
559 reveals a link between the PI3K pathway and lower estrogen-receptor (ER) levels and
560 activity in ER+ breast cancer. Breast cancer Res 2010;12:R40.
561 30 Chang WH, Forde D, Lai AG. Dual prognostic role for 2-oxoglutarate oxygenases in
562 ten diverse cancer types: Implications for cell cycle regulation and cell adhesion
563 maintenance. Cancer Commun 2019;39.
564 31 Vaupel P, Mayer A. Hypoxia in cancer: significance and impact on clinical outcome.
565 Cancer Metastasis Rev 2007;26:225–239.
566 32 Denko NC. Hypoxia, HIF1 and glucose metabolism in the solid tumour. Nat Rev
567 Cancer 2008;8:705.
568 33 Zeng W, Liu P, Pan W, et al. Hypoxia and hypoxia inducible factors in tumor
569 metabolism. Cancer Lett 2015;356:263–267.
570 34 Haider S, McIntyre A, van Stiphout RGPM, et al. Genomic alterations underlie a pan-
571 cancer metabolic shift associated with tumour hypoxia. Genome Biol 2016;17:1–17.
572 35 Korpal M, Puyang X, Wu ZJ, et al. Evasion of immunosurveillance by genomic
573 alterations of PPARγ/RXRα in bladder cancer. Nat Commun 2017;8:103.

36 Kersten S, Desvergne B, Wahli W. Roles of PPARs in health and disease. Nature 2000;405:421.

37 Wang X, Wang G, Shi Y, et al. PPAR-delta promotes survival of breast cancer cells in harsh metabolic conditions. Oncogenesis 2016;5:e232.

38 Abdollahi A, Schwager C, Kleeff J, et al. Transcriptional network governing the angiogenic switch in human pancreatic cancer. Proc Natl Acad Sci 2007;104:12890–12895.

39 Huang X-F, Han J, Hu X-T, et al. Mechanisms involved in biological behavior changes associated with Angptl4 expression in colon cancer cell lines. Oncol Rep 2012;27:1541–1547.

40 Padua D, Zhang XH-F, Wang Q, et al. TGFβ primes breast tumors for lung metastasis seeding through angiopoietin-like 4. Cell 2008;133:66–77.

41 Nakayama T, Hirakawa H, Shibata K, et al. Expression of angiopoietin-like 4 in human gastric cancer: ANGPTL4 promotes venous invasion. Oncol Rep 2010;24:599–606.

42 Nakayama T, Hirakawa H, Shibata K, et al. Expression of angiopoietin-like 4 (ANGPTL4) in human colorectal cancer: ANGPTL4 promotes venous invasion and distant metastasis. Oncol Rep 2011;25:929–935.

43 Adhikary T, Brandt DT, Kaddatz K, et al. Inverse PPARβ/δ agonists suppress oncogenic signaling to the ANGPTL4 gene and inhibit cancer cell invasion. Oncogene 2013;32:5241.

44 Shimada T, Kojima K, Yoshiura K, et al. Characteristics of the peroxisome proliferator activated receptor γ (PPARγ) ligand induced apoptosis in colon cancer cells. Gut 2002;50:658–664.

45 Leung WK, Bai AHC, Chan VYW, et al. Effect of peroxisome proliferator activated receptor γ ligands on growth and gene expression profiles of gastric cancer cells. Gut 2004;53:331–338.

46 Guo F, Ren X, Dong Y, et al. Constitutive expression of PPARγ inhibits proliferation and migration of gastric cancer cells and down-regulates Wnt/β-catenin signaling

pathway downstream target genes TERT and ENAH. Gene 2016;584:31–37.

47 Biswas SK. Metabolic reprogramming of immune cells in cancer progression. Immunity 2015;43:435–449.

48 Kidani Y, Bensinger SJ. Liver X receptor and peroxisome proliferator-activated receptor as integrators of lipid homeostasis and immunity. Immunol Rev 2012;249:72–83.

49 Li H, Sorenson AL, Poczobutt J, et al. Activation of PPARγ in myeloid cells promotes lung cancer progression and metastasis. PLoS One 2011;6:e28133.

50 Odegaard JI, Chawla A. Alternative macrophage activation and metabolism. Annu Rev Pathol Mech Dis 2011;6:275–297.

51 Park J, Lee SE, Hur J, et al. M-CSF from cancer cells induces fatty acid synthase and PPARβ/δ activation in tumor myeloid cells, leading to tumor progression. Cell Rep 2015;10:1614–1625.

52 Ma C, Kesarwala AH, Eggert T, et al. NAFLD causes selective CD4+ T lymphocyte loss and promotes hepatocarcinogenesis. Nature 2016;531:253.

53 Traversari C, Sozzani S, Steffensen KR, et al. LXR-dependent and-independent effects of oxysterols on immunity and tumor growth. Eur J Immunol 2014;44:1896–1903.

54 Lu X, Bijli KM, Ramirez A, et al. Hypoxia downregulates PPARγ via an ERK1/2-NF-κB-Nox4-dependent mechanism in human pulmonary artery smooth muscle cells. Free Radic Biol Med 2013;63:151–160.

55 Zhou J, Zhang S, Xue J, et al. Activation of peroxisome proliferator-activated receptor $α$ (PPARα) suppresses hypoxia-inducible factor-1α (HIF-1α) signaling in cancer cells. J Biol Chem 2012;287:35161–35169.

56 Narravula S, Colgan SP. Hypoxia-inducible factor 1-mediated inhibition of peroxisome proliferator-activated receptor α expression during hypoxia. J Immunol 2001;166:7543–7548.

57 Krzywinska E, Kantari-Mimoun C, Kerdiles Y, et al. Loss of HIF-1α in natural killer

cells inhibits tumour growth by stimulating non-productive angiogenesis. Nat Commun 2017;8:1597.

58 Wenes M, Shang M, Di Matteo M, et al. Macrophage metabolism controls tumor blood vessel morphogenesis and metastasis. Cell Metab 2016;24:701–715.

59 Chiu DK-C, Xu IM-J, Lai RK-H, et al. Hypoxia induces myeloid-derived suppressor cell recruitment to hepatocellular carcinoma through chemokine (C-C motif) ligand 26. Hepatology 2016;64:797–813.

642 **Figure legends:**

643

644 **Figure 1. Pan-cancer genomic alterations of PPAR pathway genes. (A)** Development of
645 an 18-gene signature consisting of putative loss- and gain-of-function genes. Somatic copy
646 number alterations and differential expression of 74 PPAR genes are investigated. Prognosis
647 of the signature is validated in six cancer cohorts. Pie slices depict the number of patients
648 within each cohort. Crosstalk between PPAR signaling, tumor hypoxia, and tumor immunity is
649 investigated. **(B)** Stacked bar chart depicts the fraction of samples within each cancer that
650 contain shallow and deep copy number alterations. The width of the bars is proportional to the
651 number of samples within each cancer type. **(C)** Somatic losses and differential expression
652 profiles of 51 genes and **(D)** somatic gains and differential expression profiles of 25 genes that
653 are recurrently deleted or amplified respectively in at least 20% of samples within each cancer
654 in at least 7 cancer types. Heatmaps on the far left show the fraction of samples in which a
655 given gene is deleted or amplified. Heatmaps in the center show differential expression values
656 between tumor and non-tumor samples. Cancer types are ordered using hierarchical
657 clustering with Euclidean distance metric. Genes that are lost and downregulated (38 genes)
658 and genes that are gained and upregulated (5 genes) are highlighted in red. Bar charts on the
659 far right depict the number of cancers harboring at least 20% of samples affected by gains
660 and losses. Refer to Table S2 for cancer abbreviations.

661

662 **Figure 2. Prognostic significance of PPAR genes. (A)** Heatmap depicts hazard ratio values
663 obtained from Cox regression analyses on 43 gain-of-function and loss-of-function candidates
664 across all cancer types. Refer to Table S2 for cancer abbreviations. **(B)** The heatmap shows
665 Spearman's correlation coefficient values comparing hazard ratios of the 43 genes. Highly
666 correlated prognostic genes are highlighted; gene names marked in blue and correlation
667 coefficients marked with a red box. **(C)** Box plot represents the distribution of 18-gene scores
668 derived from PPAR signature genes across all cancers. Cancers are ranked from high to low
669 using median scores. **(D)** Kaplan-Meier analyses of the 18-gene signature confirmed

prognosis in six cancer cohorts. Patients are stratified into the 1st and 4th quartiles based on their 18-gene scores. P values are obtained from log-rank tests. **(E)** Chord diagram shows which of the individual 18 genes harbored prognostic information in the six cohorts shown in **(D).** For example, *GK*, *PLIN5*, and *PPARG* are individually prognostic in bladder cancer. BLCA = bladder, GBMLGG = glioma, KIPAN = pan-kidney, KIRC = clear cell renal cell, LIHC = liver and STES = stomach and esophageal.

Figure 3. The 18-gene signature is independent of tumor stage. (A) Kaplan-Meier analyses of patients stratified by tumor stage or in the case of glioma by histological subtype, and the 18-gene signature. For histological subtypes of glioma, log-rank tests are used to compare patients within the 1st and 4th survival quartiles. For the other cancers, patients are first stratified according to tumor, node, and metastasis (TNM) staging followed by median-stratification into low- and high-score groups using the 18-gene signature. P values are obtained from log-rank tests. **(B)** Predictive performance of the signature is determined using receiver operating characteristic analyses. ROC curves generated using the signature are compared to those generated using a combined model uniting the signature and TNM staging. For glioma patients, the area under the curves (AUCs) for astrocytoma, oligoastrocytoma, glioblastoma multiforme and all glioma samples as a whole are shown.

Figure 4. Dysregulated PPAR signaling converges on transcriptional targets implicated in diverse metabolic processes. Differential expression analyses are performed between 4th and 1st quartile patients stratified by the 18-gene signature in six cancer cohorts. **(A)** The Venn diagram shows the number of overlapping differentially expressed genes (DEGs) in the six cohorts. DEG numbers are shown in parentheses. Functional enrichment analyses are performed by mapping DEGs to the **(B)** Gene Ontology, **(C)** KEGG and **(D)** ENCODE and ChEA databases. Enriched transcription factor binding associated with DEGs are shown in **(D)**.

Figure 5. Prognostic relevance of the crosstalk between PPAR signaling and tumor hypoxia. (A) Scatter plots show significant positive or negative correlations between 18-gene and hypoxia scores. Patients are grouped into four categories based on median 18-gene and hypoxia scores. Density plots at the x- and y-axes show the distribution of 18-gene and hypoxia scores. **(B)** Kaplan-Meier analyses are performed on the four patient groups to determine the ability of the combined PPAR-hypoxia model in determining overall survival in multiple cancers including glioma histological subtypes. P values are obtained from log-rank tests. **(C)** Table inset shows univariate Cox proportional hazards analyses of the relationship between PPAR signaling and hypoxia. Significant P values are highlighted in bold. CI = confidence interval.

Figure 6. PPAR signaling is associated with immunosuppressive phenotypes. (A) Scatter plot depicts a significant positive correlation between 18-gene and regulatory T cell (Treg) scores in glioma patients. Patients are grouped into four categories based on median 18-gene and Treg scores. Density plots at the x- and y-axes show the distribution of 18-gene and Treg scores. **(B)** Kaplan-Meier analyses are performed on the four patient groups to determine the ability of the combined PPAR-Treg model in determining overall survival in glioma histological subtypes. P values are obtained from log-rank tests. **(C)** Table inset shows univariate Cox proportional hazards analyses of the relationship between PPAR signaling and tumor immunity in glioma. Significant P values are highlighted in bold. CI = confidence interval.

Figure 7. Pan-cancer model of PPAR dysregulation and proposed crosstalk with tumor hypoxia immunity. (A) The pathway diagram represents the relationship between each of the 18 signature genes. Genes that confer good prognosis are colored in blue while genes that confer poor prognosis are colored in red. Color intensities represent the number of cancer cohorts in which a given gene is prognostic. Only six cohorts, as shown in figures 2D, 3 and 4, are considered in this diagram. **(B)** As determined in figure 5, PPAR signaling is positively or negatively correlated with tumor hypoxia depending on cellular context. **(C)** PPAR signaling

promotes immune evasion in glioma. The circular heatmap in the center represents 18-gene scores in glioma sorted in descending order with each spoke representing an individual patient. Circular heatmaps of five immune checkpoint genes are plotted with patients sorted in descending order of 18-gene scores. Spearman's correlation coefficients between 18-gene scores and immune checkpoint gene expression values are shown in the center of the heatmap.

Supplementary figure legends:

Figure S1. Crosstalk between PPAR and mTOR/PI3K/AKT signaling. (A) Kaplan-Meier analyses are performed on patients grouped into four categories based on median 18-gene PPAR and median mTOR scores to determine the ability of the combined PPAR-mTOR model in determining overall survival in patients with bladder cancer or glioma. P values are obtained from log-rank tests. **(B)** Table inset shows univariate Cox proportional hazards analyses of the relationship between PPAR and mTOR signaling. Significant P values are highlighted in bold. CI = confidence interval.

Figure S2. Heatmaps depict correlations between the expression profiles of individual PPAR signature genes and seven AMPK genes. Heatmaps were generated based on Spearman's correlation coefficient values.

Figure S3. PPAR signaling is associated with hypoxia-mediated metabolic dysregulation. (A) Scatter plot depicts a significant positive correlation between 18-gene PPAR and 44-gene-hypoxia-metabolic scores in glioma patients. Patients are grouped into four categories based on median 18-gene and 44-gene scores. Density plots at the x- and y-axes show the distribution of 18-gene and 44-gene scores. **(B)** Kaplan-Meier analysis is performed on the four patient groups to determine the ability of the combined PPAR-hypoxia-metabolism model in determining overall survival in glioma patients. P value is obtained from

log-rank test. **(C)** Table inset shows univariate Cox proportional hazards analyses of the relationship between PPAR signaling and hypoxia-associated metabolic derangements in glioma. Significant P values are highlighted in bold. CI = confidence interval.

Supplementary table legends:

Table S1. List of 74 PPAR pathway genes.

Table S2. Abbreviations and number of tumor and non-tumor samples in TCGA cancers.

Table S3. Univariate and multivariate Cox proportional hazards regression analyses to determine the independence of 18-gene signature from TNM staging.

Table S4. Differentially expressed genes between patients separated by the 18-gene signature into 4th and 1st quartiles.

Figure 1


A
74 PPAR signalling genes
21 cancer types (n=18,484)
Differential expression (Tumor vs. non-tumor)
Genomic data (Copy number variation)
Clinical data (Survival analyses)
Development of an 18-gene signature from highly correlated prognostic genes
Validation of signature
Kaplan-Meier analyses
Cox regression analyses
Six prognostic cohorts
599
408
371
669
533
889
Bladder
Glioma
Pan-kidney
Renal clear cell
Liver
Stomach & Oesophageal
Crosstalk with hypoxia and tumor immunity
Therapeutic implications
PPARα & PPARγ agonist or antagonist
Hypoxia & HIF inhibitors
Immune checkpoint blockade
B
UCEC
STES
STAD
SARC
PAAD
LUSC
LUAD
LIHC
KIRP
KIRC
KIPAN
KICH
HNSC
GBMLGG
GBM
ESCA
COAD
CHOL
CESC
BRCA
BLCA
0.00
0.25
0.50
0.75
1.00
Fraction of samples with CNV
Deep amplification
Shallow amplification
No alteration
Shallow deletion
C
Somatic deletions
Differential expression
LPL
AQP7
CPT1B
ME1
PLIN2
PPARA
SCD
ACSL1
ACSL5
FABP7
SORBS1
ACOX2
CYP8B1
FABP2
FABP3
PCK2
RXRA
SCD5
UCP1
ACAA1
APOA1
APOA5
APOC3
GK2
SLC27A2
SLC27A4
ACOX3
ACSBG2
ANGPTL4
GK
ILK
PLIN4
PLIN5
PPARG
ACSBG1
ACSL6
CPT2
CYP4A22
MMP1
SCP2
SLC27A6
ACADM
CYP4A11
FABP6
ACADL
ACSL3
CYP27A1
NR1H3
PDPK1
RXRB
SLC27A1
ESCA LUSC KICH CHOL KIPAN KIRC BLCA BRCA SARC CESC HNSC LUAD STAD STES GBM GBMLGG COAD LIHC PAAD KIRP UCEC
CHOL KIPAN KIRC SARC KICH KIRP BRCA HNSC LUAD LUSC CESC BLCA UCEC GBM GBMLGG PAAD ESCA STAD STES COAD LIHC
0 5 10 15
Number of cancers
Fraction deleted
0.2 0.4 0.6 0.8 1.0
Log2 fold change
-10 -5 0 5 10
D
Somatic amplification
Differential expression
PCK1
PLTP
CD36
CYP7A1
FABP4
FABP5
ACOX1
APOA2
RXRG
ADIPOQ
EHHADH
OLR1
PPARD
RXRB
UBC
CPT1C
PDPK1
SLC27A5
CPT1A
FABP1
ACSL4
FABP6
HMGCS2
PLIN1
RXRA
KIRP SARC PAAD UCEC GBM GBMLGG KICH KIPAN KIRC CESC HNSC LUSC BLCA ESCA COAD STAD STES CHOL LIHC BRCA LUAD
CHOL PAAD BLCA ESCA CESC UCEC GBM GBMLGG LUAD LUSC COAD STAD STES BRCA HNSC LIHC KICH SARC KIRP KIPAN KIRC
0 5 10 15 20
Number of cancers
Fraction amplified
0.2 0.4 0.6 0.8 1.0
Log2 fold change
-5 -2.5 0 2.5 5

Figure 2

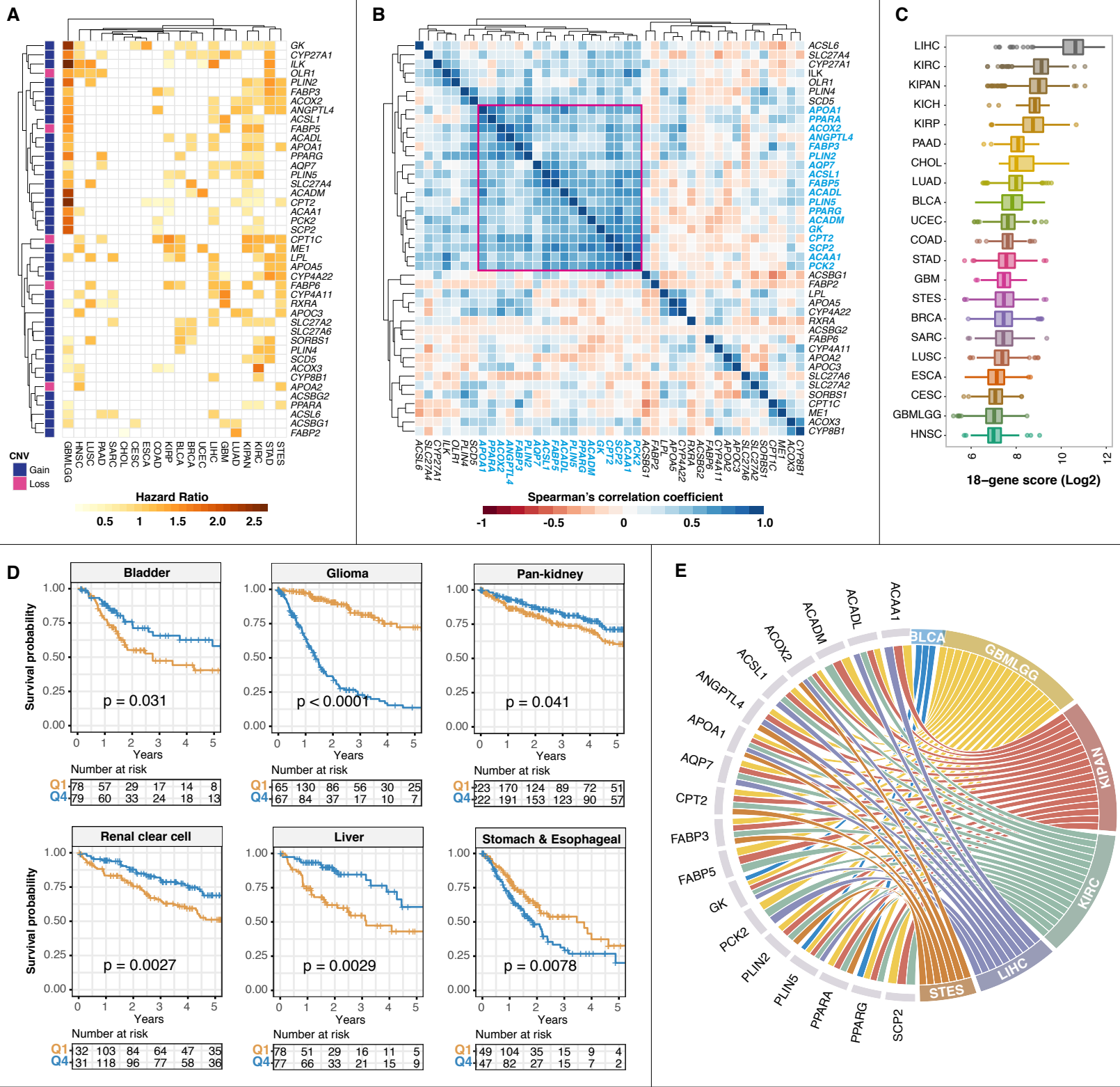
A
GK
CYP27A1
ILK
OLR1
PLIN2
FABP3
ACOX2
ANGPTL4
ACSL1
FABP5
ACADL
APOA1
PPARG
AQP7
PLIN5
SLC27A4
ACADM
CPT2
ACAA1
PCK2
SCP2
CPT1C
ME1
LPL
APOA5
CYP4A22
FABP6
CYP4A11
RXRA
APOC3
SLC27A2
SLC27A6
SORBS1
PLIN4
SCD5
ACOX3
CYP8B1
APOA2
ACSBG2
PPARA
ACSL6
ACSBG1
FABP2
GBMLGG HNSC LUSC PAAD SARC CHOL CESC ESCA COAD KIRP BLCA BRCA UCEC LIHC GBM LUAD KIPAN KIRC STAD STES
CNV
Gain
Loss
Hazard Ratio
0.5 1 1.5 2.0 2.5
B
ACSL6
SLC27A4
CYP27A1
ILK
OLR1
PLIN4
SCD5
APOA1
PPARA
ACOX2
ANGPTL4
FABP3
PLIN2
AQP7
ACSL1
FABP5
ACADL
PLIN5
PPARG
ACADM
GK
CPT2
SCP2
ACAA1
PCK2
ACSBG1
FABP2
LPL
APOA5
CYP4A22
RXRA
ACSBG2
FABP6
CYP4A11
APOA2
APOC3
SLC27A6
SLC27A2
SORBS1
CPT1C
ME1
ACOX3
CYP8B1
Spearman's correlation coefficient
-1 -0.5 0 0.5 1.0
C
LIHC
KIRC
KIPAN
KICH
KIRP
PAAD
CHOL
LUAD
BLCA
UCEC
COAD
STAD
GBM
STES
BRCA
SARC
LUSC
ESCA
CESC
GBMLGG
HNSC
6 8 10 12
18–gene score (Log2)
D
Bladder
p = 0.031
Glioma
p < 0.0001
Pan-kidney
p = 0.041
Renal clear cell
p = 0.0027
Liver
p = 0.0029
Stomach & Esophageal
p = 0.0078
Survival probability
Years
Number at risk
Q1 78 57 29 17 14 8
Q4 79 60 33 24 18 13
Q1 65 130 86 56 30 25
Q4 67 84 37 17 10 7
Q1 223 170 124 89 72 51
Q4 222 191 153 123 90 57
Q1 32 103 84 64 47 35
Q4 31 118 96 77 58 36
Q1 78 51 29 16 11 5
Q4 77 66 33 21 15 9
Q1 49 104 35 15 9 4
Q4 47 82 27 15 7 2
E
ACAA1
ACADL
ACADM
ACOX2
ACSL1
ANGPTL4
APOA1
AQP7
CPT2
FABP3
FABP5
GK
PCK2
PLIN2
PLIN5
PPARA
PPARG
SCP2
BLCA
GBMLGG
KIPAN
KIRC
LIHC
STES

Figure 3

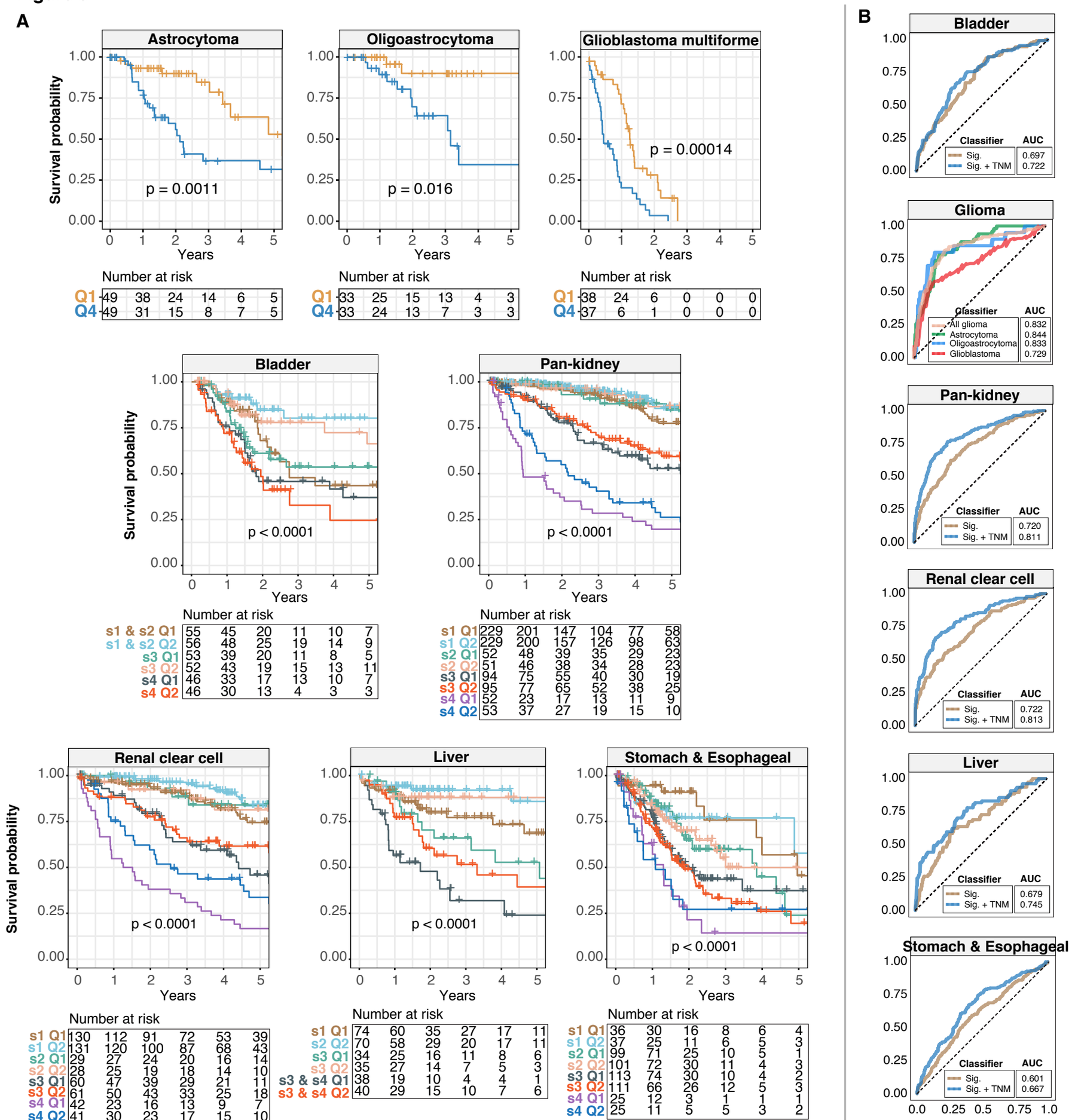
A
Astrocytoma
p = 0.0011
Oligoastrocytoma
p = 0.016
Glioblastoma multiforme
p = 0.00014
Survival probability
Years
Number at risk
Q1 49 38 24 14 6 5
Q4 49 31 15 8 7 5
Q1 33 25 15 13 4 3
Q4 33 24 13 7 3 3
Q1 38 24 6 0 0 0
Q4 37 6 1 0 0 0
Bladder
p < 0.0001
Pan-kidney
p < 0.0001
s1 & s2 Q1 55 45 20 11 10 7
s1 & s2 Q2 56 48 25 19 14 9
s3 Q1 53 39 20 11 8 5
s3 Q2 52 43 19 15 13 11
s4 Q1 46 33 17 13 10 7
s4 Q2 46 30 13 4 3 3
s1 Q1 229 201 147 104 77 58
s1 Q2 229 200 157 126 98 63
s2 Q1 52 48 39 35 29 23
s2 Q2 51 46 38 34 28 23
s3 Q1 94 75 55 40 30 19
s3 Q2 95 77 65 52 38 25
s4 Q1 52 23 17 13 11 9
s4 Q2 53 37 27 19 15 10
Renal clear cell
p < 0.0001
Liver
p < 0.0001
Stomach & Esophageal
p < 0.0001
s1 Q1 130 112 91 72 53 39
s1 Q2 131 120 100 87 68 43
s2 Q1 29 27 24 20 16 14
s2 Q2 28 25 19 18 14 10
s3 Q1 60 47 39 29 21 11
s3 Q2 61 50 43 33 25 18
s4 Q1 42 23 16 13 9 7
s4 Q2 41 30 23 17 15 10
s1 Q1 74 60 35 27 17 11
s2 Q2 70 58 29 20 17 11
s3 Q1 34 25 16 11 8 6
s3 Q2 35 27 14 7 5 3
s3 & s4 Q1 38 19 10 4 4 1
s3 & s4 Q2 40 29 15 10 7 6
s1 Q1 36 30 16 8 6 4
s1 Q2 37 25 11 6 5 3
s2 Q1 99 71 25 10 5 1
s2 Q2 101 72 30 11 4 3
s3 Q1 113 74 30 10 4 2
s3 Q2 111 66 26 12 5 3
s4 Q1 25 12 3 1 1 1
s4 Q2 25 11 5 5 3 2
B
Bladder
Classifier AUC
Sig. 0.697
Sig. + TNM 0.722
Glioma
Classifier AUC
All glioma 0.832
Astrocytoma 0.844
Oligoastrocytoma 0.833
Glioblastoma 0.729
Pan-kidney
Classifier AUC
Sig. 0.720
Sig. + TNM 0.811
Renal clear cell
Classifier AUC
Sig. 0.722
Sig. + TNM 0.813
Liver
Classifier AUC
Sig. 0.679
Sig. + TNM 0.745
Stomach & Esophageal
Classifier AUC
Sig. 0.601
Sig. + TNM 0.667

Figure 4

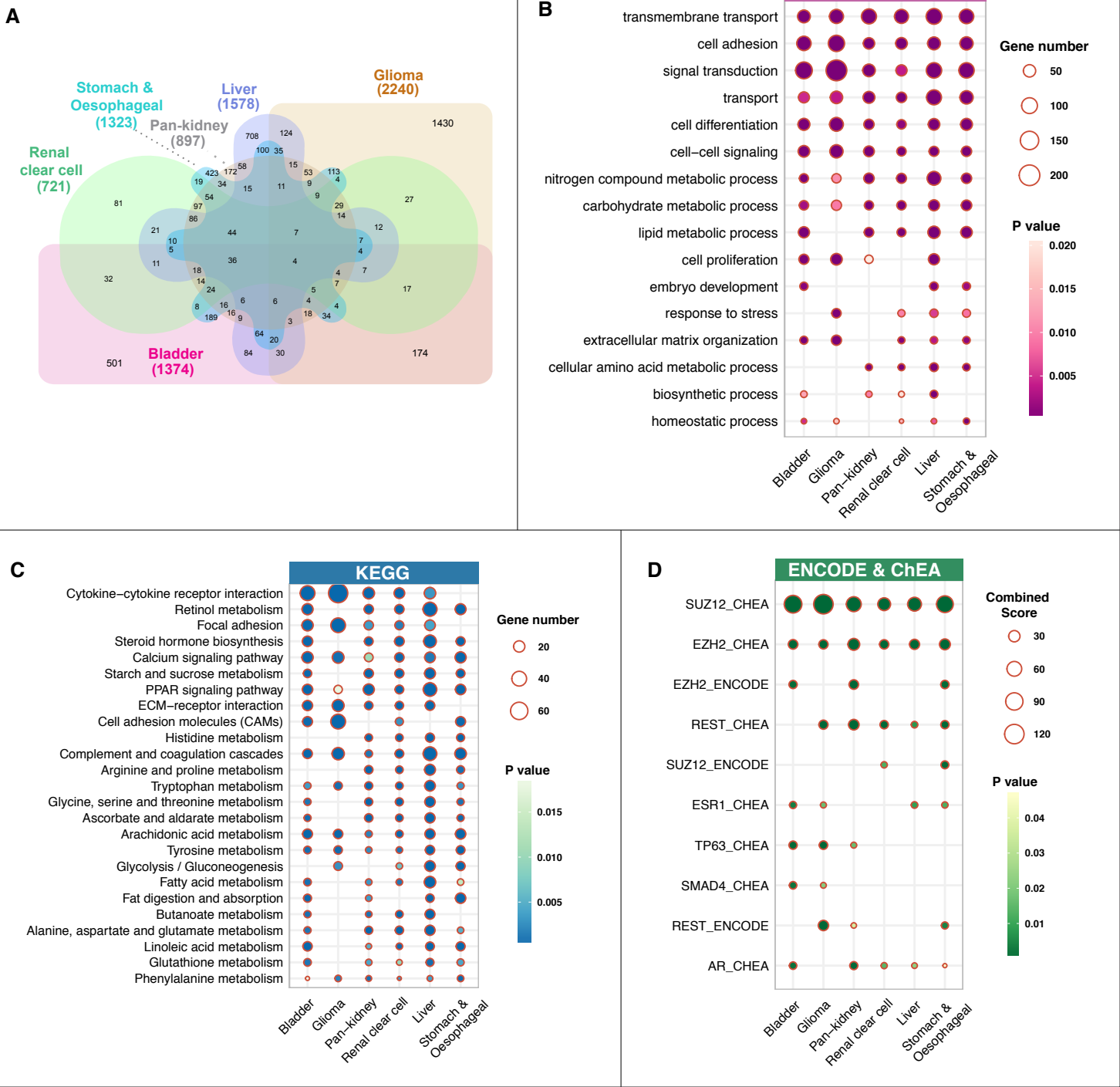
A
Stomach & Oesophageal (1323)
Liver (1578)
Glioma (2240)
Pan-kidney (897)
Renal clear cell (721)
Bladder (1374)
1430
81
27
32
17
501
174
B
Gene Ontology
transmembrane transport
cell adhesion
signal transduction
transport
cell differentiation
cell–cell signaling
nitrogen compound metabolic process
carbohydrate metabolic process
lipid metabolic process
cell proliferation
embryo development
response to stress
extracellular matrix organization
cellular amino acid metabolic process
biosynthetic process
homeostatic process
Bladder
Glioma
Pan–kidney
Renal clear cell
Liver
Stomach & Oesophageal
Gene number
50
100
150
200
P value
0.020
0.015
0.010
0.005
C
KEGG
Cytokine–cytokine receptor interaction
Retinol metabolism
Focal adhesion
Steroid hormone biosynthesis
Calcium signaling pathway
Starch and sucrose metabolism
PPAR signaling pathway
ECM–receptor interaction
Cell adhesion molecules (CAMs)
Histidine metabolism
Complement and coagulation cascades
Arginine and proline metabolism
Tryptophan metabolism
Glycine, serine and threonine metabolism
Ascorbate and aldarate metabolism
Arachidonic acid metabolism
Tyrosine metabolism
Glycolysis / Gluconeogenesis
Fatty acid metabolism
Fat digestion and absorption
Butanoate metabolism
Alanine, aspartate and glutamate metabolism
Linoleic acid metabolism
Glutathione metabolism
Phenylalanine metabolism
Bladder
Glioma
Pan–kidney
Renal clear cell
Liver
Stomach & Oesophageal
Gene number
20
40
60
P value
0.015
0.010
0.005
D
ENCODE & ChEA
SUZ12_CHEA
EZH2_CHEA
EZH2_ENCODE
REST_CHEA
SUZ12_ENCODE
ESR1_CHEA
TP63_CHEA
SMAD4_CHEA
REST_ENCODE
AR_CHEA
Bladder
Glioma
Pan–kidney
Renal clear cell
Liver
Stomach & Oesophageal
Combined Score
30
60
90
120
P value
0.04
0.03
0.02
0.01

Figure 5

A

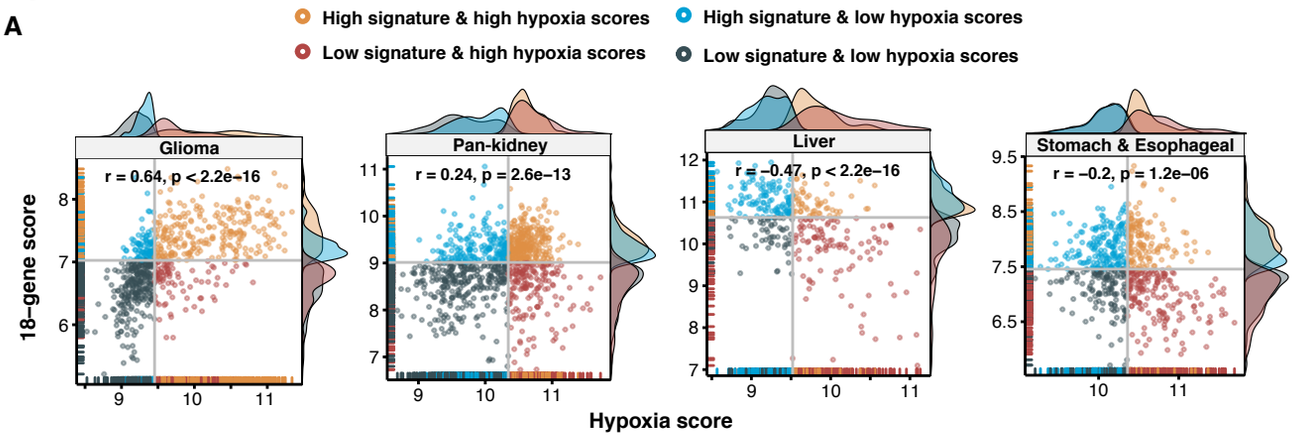

B

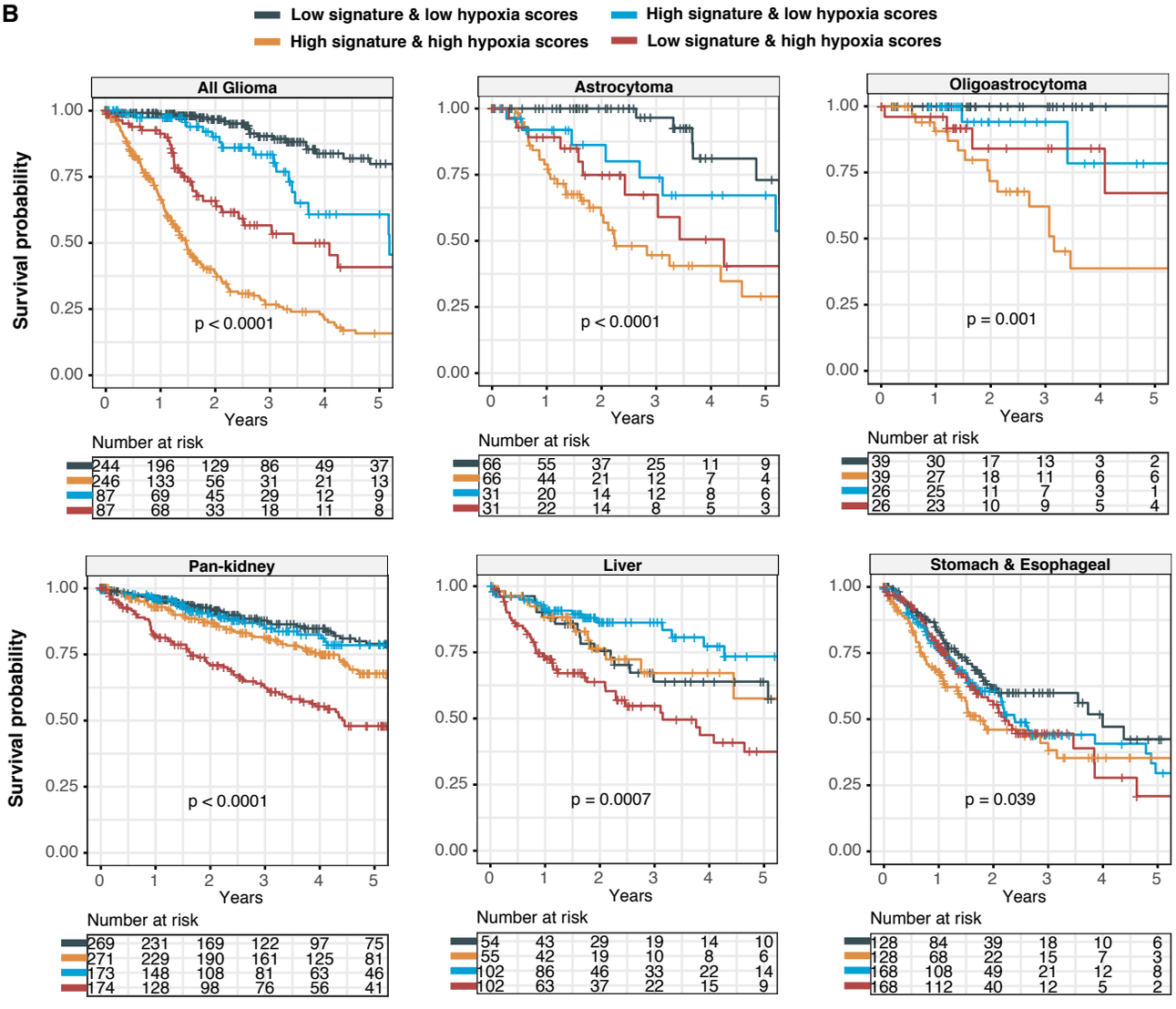

C

	Hazard Ratio (95% CI)	*P*-value
Glioma		
High signature & high hypoxia scores vs. low signature & low hypoxia scores	7.938 (5.509 - 11.437)	**< 0.0001**
High signature & low hypoxia scores vs. low signature & low hypoxia scores	1.879 (1.086 - 3.251)	**0.024**
Low signature & high hypoxia scores vs. low signature & low hypoxia scores	3.011 (1.863 - 4.868)	**< 0.0001**
Astrocytoma		
High signature & high hypoxia scores vs. low signature & low hypoxia scores	7.380 (3.218 - 16.920)	**< 0.0001**
High signature & low hypoxia scores vs. low signature & low hypoxia scores	3.027 (1.123 - 8.160)	**0.028**
Low signature & high hypoxia scores vs. low signature & low hypoxia scores	3.964 (1.528 - 10.290)	**0.0046**
Oligoastrocytoma		
High signature & high hypoxia scores vs. low signature & low hypoxia scores	14.179 (2.871 - 20.490)	**0.011**
High signature & low hypoxia scores vs. low signature & low hypoxia scores	2.963 (0.268 - 22.720)	0.38
Low signature & high hypoxia scores vs. low signature & low hypoxia scores	5.442 (0.626 - 27.300)	0.12
Pan-kidney		
High signature & high hypoxia scores vs. high signature & low hypoxia scores	1.558 (1.016 - 2.389)	**0.042**
Low signature & low hypoxia scores vs. high signature & low hypoxia scores	0.896 (0.558 - 1.440)	0.65
Low signature & high hypoxia scores vs. high signature & low hypoxia scores	3.187 (2.083 - 4.878)	**< 0.0001**
Liver		
High signature & high hypoxia scores vs. high signature & low hypoxia scores	1.608 (0.816 - 3.169)	0.17
Low signature & low hypoxia scores vs. high signature & low hypoxia scores	1.611 (0.837 - 3.101)	0.15
Low signature & high hypoxia scores vs. high signature & low hypoxia scores	2.849 (1.664 - 4.878)	**0.00014**
Stomach & Esophageal		
High signature & high hypoxia scores vs. low signature & low hypoxia scores	1.748 (1.175 - 2.600)	**0.0058**
High signature & low hypoxia scores vs. low signature & low hypoxia scores	1.304 (0.892 - 1.907)	0.17
Low signature & high hypoxia scores vs. low signature & low hypoxia scores	1.381 (0.937 - 2.033)	0.11

Figure 6

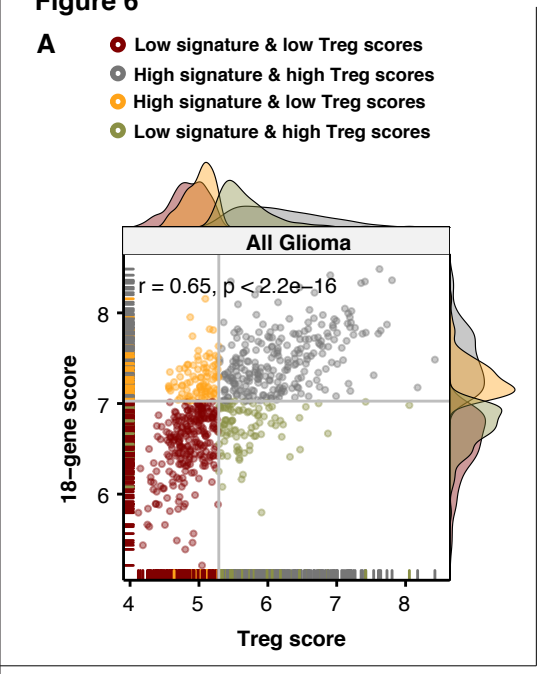

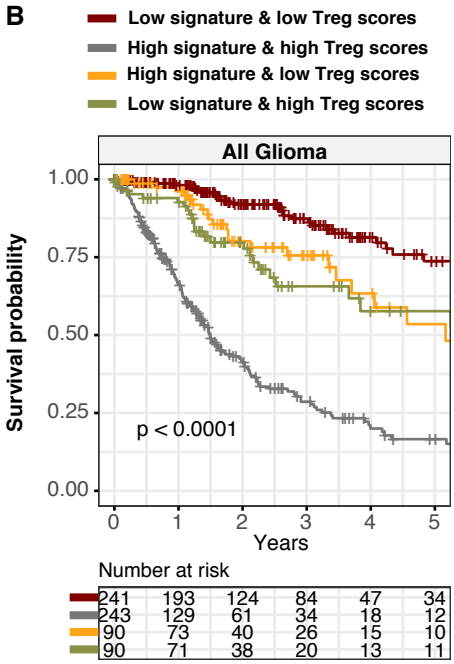

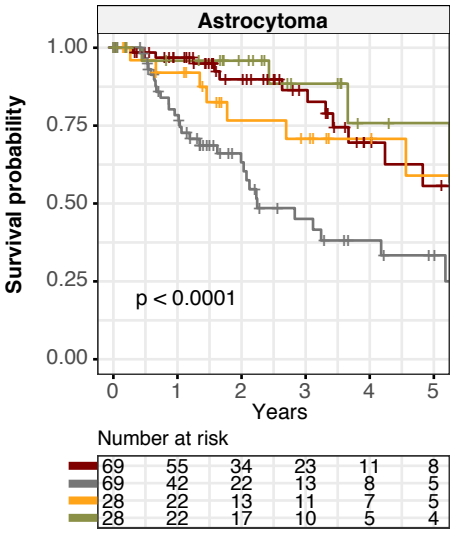

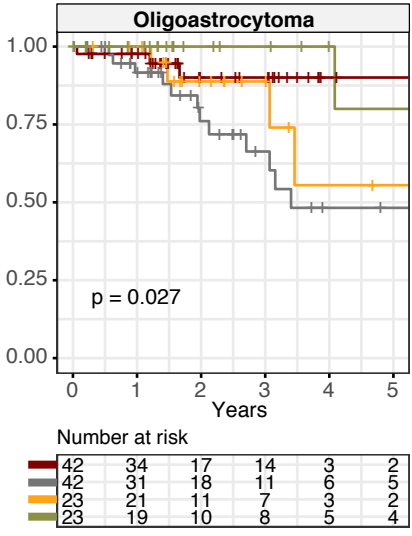

C

	Hazard Ratio (95% CI)	*P*-value
Glioma		
High signature & high Treg scores vs. low signature & low Treg scores	7.356 (5.165 - 10.478)	**< 0.0001**
High signature & low Treg scores vs. low signature & low Treg scores	1.872 (1.128 - 3.107)	**0.016**
Low signature & high Treg scores vs. low signature & low Treg scores	2.255 (1.386 - 3.671)	**0.00011**
Astrocytoma		
High signature & high Treg scores vs. low signature & low Treg scores	3.699 (1.937 - 7.062)	**< 0.0001**
High signature & low Treg scores vs. low signature & low Treg scores	1.383 (0.592 - 3.233)	0.45
Low signature & high Treg scores vs. low signature & low Treg scores	0.599 (0.196 - 1.830)	0.37
Oligoastrocytoma		
High signature & high Treg scores vs. low signature & low Treg scores	3.227 (1.059 - 9.830)	**0.038**
High signature & low Treg scores vs. low signature & low Treg scores	1.697 (0.422 - 6.826)	0.46
Low signature & high Treg scores vs. low signature & low Treg scores	0.627 (0.113 - 3.480)	0.59

Figure 7

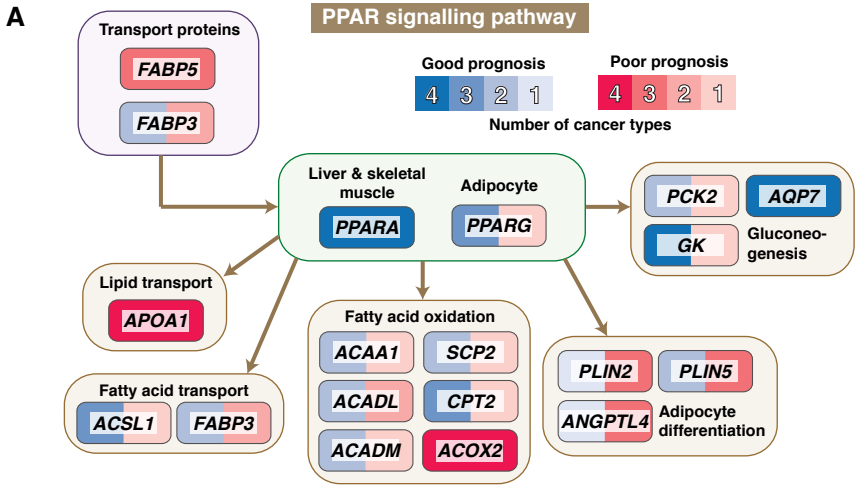
A
PPAR signalling pathway
Transport proteins
FABP5
FABP3
Good prognosis
4 3 2 1
Poor prognosis
4 3 2 1
Number of cancer types
Liver & skeletal muscle
PPARA
Adipocyte
PPARG
PCK2
AQP7
GK
Gluconeo-genesis
Lipid transport
APOA1
Fatty acid oxidation
ACAA1
SCP2
ACADL
CPT2
ACADM
ACOX2
PLIN2
PLIN5
ANGPTL4
Adipocyte differentiation
Fatty acid transport
ACSL1
FABP3

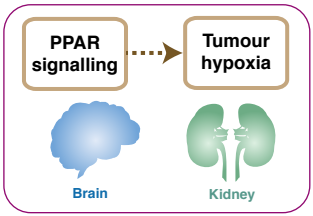
B
PPAR ~ hypoxia crosstalk
PPAR signalling
Tumour hypoxia
Brain
Kidney
PPAR signalling
Tumour hypoxia
Stomach
Liver

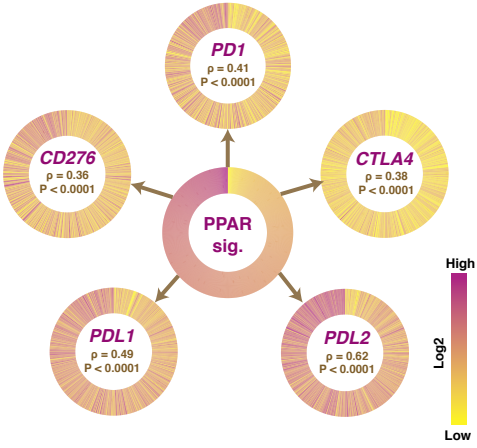
C
PPAR promotes immunosuppression
PD1
ρ = 0.41
P < 0.0001
CD276
ρ = 0.36
P < 0.0001
CTLA4
ρ = 0.38
P < 0.0001
PPAR sig.
PDL1
ρ = 0.49
P < 0.0001
PDL2
ρ = 0.62
P < 0.0001
High
Log2
Low